arXiv:1703.02207v1 [astro-ph.GA] 7 Mar 2017

The surprisingly large dust and gas content of quiescent galaxies at $z > 1.4$

R. Gobat, E. Daddi, G. Magdis, F. Bournaud, M. Sargent, M. Martig, S. Jin, A. Finoguenov, M. Béthermin, H.S. Hwang, A. Renzini, G.W. Wilson, I. Aretxaga, M. Yun, V. Strazzullo, F. Valentino

Early type galaxies (ETG) contain most of the stars present in the local Universe and, above a stellar mass of $\sim 5 \times 10^{10}$ $M_\odot$, vastly outnumber spiral galaxies like the Milky Way. These massive spheroidal galaxies have, in the present day, very little gas or dust (Lianou et al., 2016), and their stellar populations have been evolving passively for over 10 billion years. The physical mechanisms that led to the termination of star formation in these galaxies and depletion of their interstellar medium remain largely conjectural. In particular, there are currently no direct measurements of the amount of residual gas that might be still present in newly quiescent spheroids at high redshift (Sargent et al., 2015). Here we show that quiescent ETGs at $z \sim 1.8$, close to their epoch of quenching, contained $2-3$ orders of magnitude more dust at fixed stellar mass than local ETGs. This implies the presence of substantial amounts of gas ($5-10\%$), which was however consumed less efficiently than in more active galaxies, probably due to their spheroidal morphology, and consistently with our simulations. This lower star formation efficiency, and an extended hot gas halo possibly maintained by persistent feedback from an active galactic nucleus (AGN), combine to keep ETGs mostly passive throughout cosmic time.

The presence of quiescent galaxies, with very low relative rates of star formation (SFR), has been established up to $z \sim 3$ (Gobat et al., 2012; Glazebrook et al., 2017). Their existence a mere 2 Gyr after the Big Bang implies that, in at least some regions of the Universe, the processes responsible for the cessation of star formation were already very efficient. The termination of star formation in ETGs is usually attributed to the removal of cool gas reservoirs (e.g., by stellar or quasar feedback; Di Matteo et al., 2005) and/or by the suppression of gas infall and cooling (e.g., by virial shocks or AGN feedback; Birnboim & Dekel, 2003; Croton et al., 2006). Alternatively, the growth of bulges and stellar spheroids is thought to stabilise gas reservoirs, making star formation inefficient compared to disk galaxies (Martig et al., 2009; Tacchella et al., 2015). If the latter plays an important role in galaxy quenching, we might expect significant reservoirs of untapped gas to exist in galaxies that have recently turned quiescent. Detecting this residual gas at high redshift, close to the epoch of quenching for massive quiescent galaxies, is however very challenging (Sargent et al., 2015) and all attempts have so far been unsuccessful.

Deep survey fields allow us to circumnavigate this issue. By combining data from large numbers of undetected quiescent galaxies, their average far-infrared (FIR) emission can be observed, which traces the cold dust present in their interstellar medium (ISM) and, indirectly, their SFR. We select 977 isolated, high-mass ($\langle M_\star \rangle = 1.1 \times 10^{11}$ $M_\odot$) quiescent galaxies in the 2 deg^2 COSMOS field by combining two different photometric criteria (BzK and UVJ; Daddi et al., 2004; Wuyts et al., 2007) and keeping only objects that are individually undetected at mid-infrared (MIR) wavelengths (Methods). These criteria ensure that the sample contains only the least star-forming galaxies at $z = 1.4 - 2.5$, with clear early-type morphologies (as implied by a high median Sérsic index $n \sim 3.5$; Methods). We extract cutouts centred at the position of each galaxy from the 24μm (MIR), $100 - 500\mu$m (FIR), $0.85 - 1.1$ mm (sub-millimetre; sub-mm), and 20 cm (radio) observations of COSMOS and perform a median stacking analysis at each wavelength. After correcting for the contribution from satellite galaxies and unassociated neighbours in the line of sight (Methods), we obtain a clean measure of the FIR and radio emission of the quiescent galaxies, with detections in all but two bands (100 and 160μm) ranging in significance from 3.5σ to 11.9σ (Figure 1).

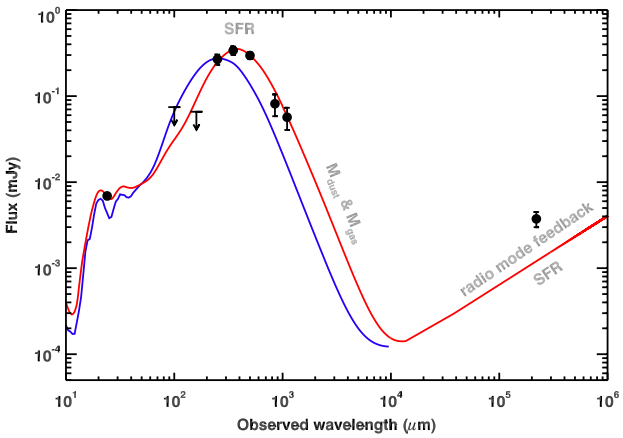

Figure 1: Mid-infrared to radio SED of 24 μm-undetected pBzK+UVJp galaxies, from stacked cutout images (filled circles, the arrows representing 3σ upper limits), with best-fit model from Draine & Li (2007, solid red curve extending to the radio regime; Methods). For comparison, the "best-fit" standard MS template (Magdis et al., 2012), which has hotter dust, is shown in blue. Both models have been broadened using the redshift distribution of the sample as kernel. The error bars on the MIR, FIR, and radio fluxes show the bootstrap uncertainties derived from the stack.

We model the cold dust emission (Draine & Li, 2007, Methods), sampling its peak ($\sim$150 μm rest-frame) and Rayleigh-Jeans tail ($> 400\mu$m rest-frame; Figure 1), which allows for an accurate determination of the dust temperature $T_{\rm dust}$ and mass $M_{\rm dust}$. The observed cold dust emission of the $z \sim 1.76$ ETG sample implies a luminosity of $L_{\rm IR} = 2.9 \pm 0.9 \times 10^{10}$ $L_\odot$ and $M_{\rm dust} = 1^{+0.6}_{-0.4} \times 10^8$ $M_\odot$. The temperature of the cold dust component, $T_{\rm dust} \sim 21 - 25$ K, as suggested by the lack of detection at $\sim 100 - 160$ μm but not at ≥ 250 μm, is similarly up to 10 K lower than the main sequence of star formation (MS) at the same $L_{\rm IR}$ (Hwang et al., 2010), among the lowest values at any redshift. This low temperature also confirms that the measured FIR emission

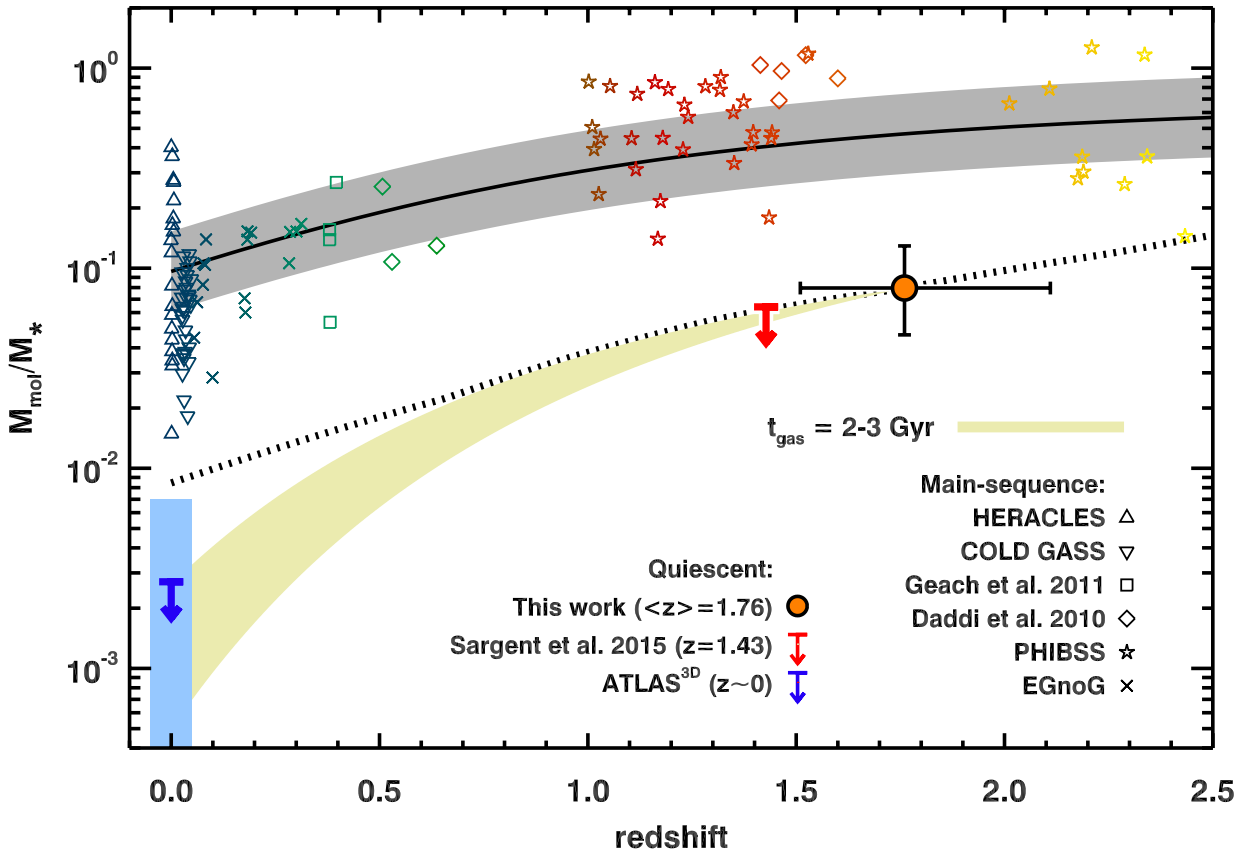

Figure 2: Evolution of the molecular gas fraction $M_{mol}/M_\star$ as a function of redshift for both quiescent and MS galaxies. The latter include low-redshift MS galaxies from the HERACLES and COLD GASS (DR1) surveys (Leroy et al., 2008; Saintonge et al., 2011), intermediate-redshift MS galaxies from EGnoG (Bauermeister et al., 2013) and Geach et al. (2011), as well as $z > 1$ MS galaxies from Daddi et al. (2010), PHIBSS (Tacconi et al., 2013), and Magdis et al. (2012). The distant ETG sample is shown by an orange dot and the upper limit constraints from CO(2-1) observations of a massive ETG at a similar redshift (Sargent et al., 2015) by a red arrow. The blue arrow marks the median upper limit on this ratio for ETGs in the ATLAS^{3D} survey, with the light blue shaded region showing the range of values for the detected subsample (22%) of ATLAS^{3D}. The black curve and grey strip show the evolution of an average MS galaxy (Sargent et al., 2014) with stellar mass 5×10^{10} M$_\odot$, and a 0.2 dex scatter approximately corresponding to the 1σ scatter of the MS. The thick dotted line shows the Sargent et al. (2014) relation offset by a factor ~ 6 and for a stellar mass of $\log M^\star(z) + \Delta M$, where ΔM is the offset between the median mass of the total pBzk+UVJp sample and the $M^\star$ of the stellar mass function of quiescent galaxies at the median redshift of the sample. Finally, the green-yellow region shows gas consumption in the closed box case (no gas inflow or outflow), with a timescale t_{gas} between 2 and 3 Gyr (lower and upper edge, respectively).

does not originate from star forming satellites, which would have T_{dust} values closer to the MS (Methods). These distant ETGs appear however to be much more dust rich than their local counterparts, with $(M_{dust}/M_\star)_{z=1.76} \sim 8 \times 10^{-4}$ compared to $(M_{dust}/M_\star)_{z=0} \gtrsim 10^{-6}$ (Smith et al., 2012) in this mass range, a difference of up to 3 orders of magnitude. We convert the measured dust mass into a gas mass assuming a gas-phase metallicity close to the solar value and a metallicity-dependent gas-to-dust ratio (Magdis et al., 2012), which yields $M_{gas} = 9.5^{+5.6}_{-3.5} \times 10^9$ M$_\odot$ (Methods). Quiescent galaxies in the nearby Universe, when they have substantial amounts of hydrogen gas, have it mostly in molecular form (Crocker et al., 2011). We thus assume that distant quiescent galaxies are similar to their local counterparts in this regard and that M_{gas} hereafter refers to molecular hydrogen rather than the combined neutral and H_2 gas mass.

The large amount of dust we detect, and the inferred gas mass, implies that high redshift ETGs are remarkably gas rich, with up to 11% of their baryonic mass being in the form of gas. As with the dust fraction, this represents an increase of more than two orders of magnitude with respect to the local Universe (Figure 2; Lianou et al., 2016), and a cosmic evolution that vastly exceeds the similar increase in the gas fraction of SF galaxies. In "normal" SF galaxies, the FIR and sub-mm emission is a relatively pure tracer of star formation. If the observed cold dust emission does indeed arise from star formation activity, converting (Kennicutt, 1998) L_{IR} into a SFR then yields $4.8^{+1.8}_{-1.3}$ M$_\odot$ yr^{-1}, in excellent agreement with the SFR of $z \sim 1.5$ ETGs derived from optical spectroscopic diagnostics (Gobat et

al., 2017), which probe different timescales (a few tens of Myr for spectroscopic line emission, several times that for FIR emission). Given the large stellar mass of these galaxies, it implies that the distant ETGs have a sSFR that is a factor ~ 30 lower than that of active galaxies on the MS at the same epoch (Figure 3). The presence of both such large gas reservoirs and a strongly suppressed SFR would imply that the star formation efficiency (SFE) of these quiescent galaxies is $2-3$ times lower than that of disk galaxies and comparable to that of local ETGs (Figure 3; Saintonge et al., 2012). This value is conservative and thus could be even lower, if part of the FIR emission of these distant ETGs arises from, e.g., heating of cirrus dust by old stellar population. Nonetheless, the good agreement between optical and IR-based SFRs further suggests that it is produced by residual star formation rather than other mechanisms. A low SFE is also consistent with the low dust temperature and small value of the dust-mass weighted luminosity $\langle U \rangle$ estimated from the IR SED, since the intensity of the radiation field can be related to the SFE and metallicity by the relation $\langle U \rangle \propto \mathrm{SFE}/Z$ (Magdis et al., 2012; Béthermin et al., 2015). It also implies a longer gas consumption timescale, $t_{\rm gas} = 2-3$ Gyr compared to $\lesssim 1$ Gyr for MS galaxies. The difference between the gas fractions of local and distant ETGs, as well as between their sSFRs, can then in principle be accounted for by the low-efficiency conversion of the residual gas into stars, while only increasing the stellar mass of the galaxy by a small fraction (Figure 2). This low efficiency in ETGs is predicted by numerical simulations (Martig et al., 2009, 2012, Methods), where the SFE decreases by a factor $5-10$ once the gas fraction drops below $20-25\%$ (Figure 4). This effect is linked to the presence of the spheroidal stellar component which, unlike a stellar disk, does not destabilise the gas disk. Conversely, in galaxies containing more than $\sim 25\%$ of gas, regardless of their stellar structure, the gas remains unstable and capable of forming stars efficiently.

Our observations suggest that this process does indeed occur in high-redshift ETGs once the gas fraction has been reduced enough, and that the suppression of star formation thus does not require the complete removal of cool gas reservoirs. However, several channels exist through which these galaxies could have been replenished with gas. Given ETGs ages of < 3 Gyr inferred from spectroscopy (Gobat et al., 2017), we can estimate that $\sim 4 \times 10^{10}$ $\mathrm{M}_\odot$ of gas were already returned to the ISM as metal enriched gas by stellar evolution, at a rate of $\lesssim 2.9$ $\mathrm{M}_\odot$ yr^{-1} at $z = 1.76$, with another $\sim 10^{10}$ $\mathrm{M}_\odot$ produced over the next 10 Gyr assuming passive evolution (Methods). Gas is also expected to be reaccreted through mergers with gas-rich satellite galaxies and through the cosmic web. This suggests that there must exist other processes to keep the cold gas fraction low in these ETGs for the rest of their cosmic evolution, either by efficiently removing the surplus gas or preventing it from cooling. There are three likely such "maintenance" mechanisms: first, the host halos of these distant ETGs are, at $\gtrsim 10^{13}$ $\mathrm{M}_\odot$, already massive enough to support a hot atmosphere, as evidenced by X-ray stacking (Methods). This hot gas can efficiently prevent the infall of cold gas onto the central galaxy (Birnboim & Dekel, 2003). The X-rays emitted by the halo can also remove, on short timescales and through sputtering (Arimoto et al., 1997), the dust produced by stellar evolution, thus contributing to the evolution of the dust content of ETGs between $z > 1.4$ and $z = 0$. Second, the "radio-mode" feedback from AGN-driven jets (as tantalizingly suggested by the systematic, $\sim 5 \times 10^{22}$ W/Hz, factor of 3 radio excess – that would imply a duty cycle of nearly 1, as opposed to 1% locally; Figure 1) can not only heat the halo gas but also drive away a fraction of the cold gas reservoir at a continuous rate (Croton et al., 2006). Finally, gravitational interaction between satellites and the halo can also provide a source of heating for the gas (Johansson, Naab & Ostriker, 2009).

The large amounts of dust we detect in our $z > 1.4$ sample, through its FIR emission, implies similarly large quantities of molecular hydrogen. This H_2 gas would thus appear to be abundant enough in these galaxies to be detectable with the Atacama Large Millimeter Array (ALMA) through sub-mm line tracers, although the confirmation of even a single galaxy can be expected to require several hours of observation. Nevertheless, our result indicates that semi-direct studies of gas in high-redshift quiescent galaxies are already marginally feasible, although the large time expenditure required and still-unknown dependencies of the dust and gas fractions on stellar mass or environment could make their design challenging.

References

Arimoto, N., Matsushita, K., Ishimaru, Y., Ohashi, T., Renzini, A., The Iron Discrepancy in Elliptical Galaxies after ASCA, Astrophys. J. 477, 128 (1997)

Bauermeister, A. et al., The EGNoG Survey: Molecular Gas in Intermediate-Redshift Star-Forming Galaxies, Astrophys. J. 768, 132 (2013)

Béthermin, M. et al., Evolution of the dust emission of massive galaxies up to $z = 4$ and constraints on their dominant mode of star formation, Astron. Astrophys. 573, 113 (2015)

Birnboim, Y, Dekel, A., Virial shocks in galactic haloes?, Mon. Not. R. Astron. Soc. 345, 349 (2003)

Boselli, A. et al., Cold gas properties of the Herschel Reference Survey. II. Molecular and total gas scaling relations, Astron. Astrophys. 564, 65 (2014)

Crocker, A.F., Bureau, M., Young., L.M., Combes, F., Molecular gas and star formation in early-type galaxies, Mon. Not. R. Astron. Soc. 410, 1197 (2011)

Croton, D.J. et al., The many lives of active galactic nuclei: cooling flows, black holes and the luminosities and colours of galaxies, Mon. Not. R. Astron. Soc. 2006, 365, 11

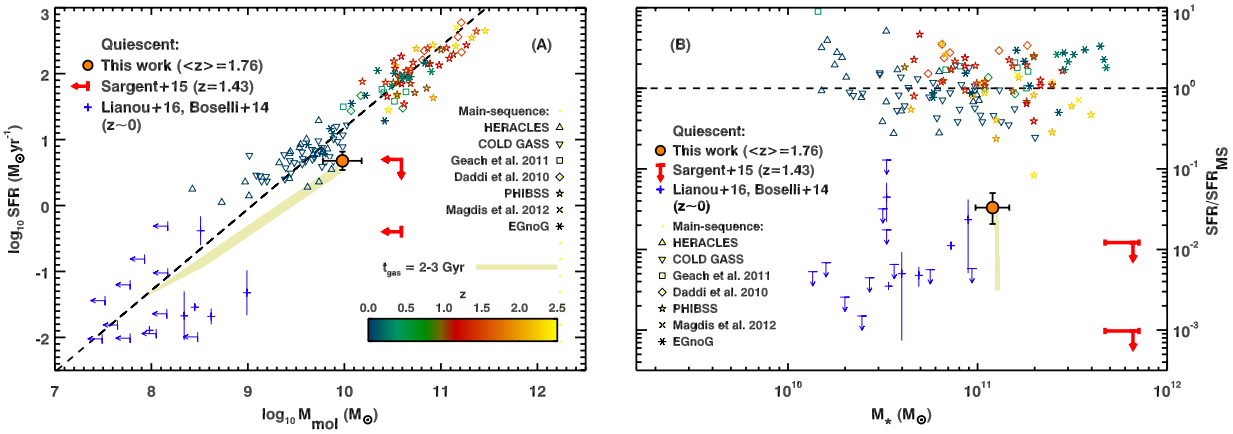

Figure 3: *A):* correlation between the molecular gas content and SFR of galaxies, including the same MS samples as in Fig. 2. Our median measurement, shown as a orange filled circle with error bars, is offset by $\sim 3\sigma$ from the average SFR $-$ $M_{\rm mol}$ relation for MS galaxies (black dashed line, as parameterised in Sargent et al., 2014). For comparison, the upper limit constraints from CO(2-1) observations of a massive ETG at a similar redshift (Sargent et al., 2015) is shown by red arrows and the low redshift ETG measurements from Boselli et al. (2014) and Lianou et al. (2016) are shown as blue crosses and arrows (in the case of upper limits on $M_{\rm mol}$). The green-yellow region shows the same closed-box evolution from $z = 1.76$ to $z = 0$, as in Figure 2. *B):* SFR of star forming and quiescent galaxies as a fraction of the MS one, for the same data as in *A)*.

Daddi, E. et al., A New Photometric Technique for the Joint Selection of Star-forming and Passive Galaxies at $1.4 \lesssim z \lesssim 2.5$, Astrophys. J. 617, 746 (2004)

Daddi, E. et al., Different Star Formation Laws for Disks Versus Starbursts at Low and High Redshifts, Astrophys. J. Let. 714, 118 (2010)

Di Matteo, T., Springel, V., Hernquist, L., Energy input from quasars regulates the growth and activity of black holes and their host galaxies, Nature 433, 604 (2005)

Draine, B.T., Li, A., Infrared Emission from Interstellar Dust. IV. The Silicate-Graphite-PAH Model in the Post-Spitzer Era, Astrophys. J. 657, 810 (2007)

Geach, J.E. et al., On the Evolution of the Molecular Gas Fraction of Star-Forming Galaxies, Astrophys. J. Let. 730, 19 (2011)

Glazebrook, K. et al., A massive, quiescent galaxy at redshift of $z = 3.717$, Nature, arXiv:1702.01751

Gobat, R. et al., The Early Early Type: Discovery of a Passive Galaxy at $z_{\rm spec} \sim 3$, Astrophys. J. Let. 759, 44 (2012)

Gobat, R. et al., In and out star formation in $z \sim 1.5$ quiescent galaxies from rest-frame UV spectroscopy and the far-infrared, Astron. Astrophys., arXiv:1612.06955

Hwang, H.S. et al., Evolution of dust temperature of galaxies through cosmic time as seen by Herschel, Mon. Not. R. Astron. Soc. 409, 75 (2010)

Johansson, P.H., Naab, T., Ostriker, J.P., Gravitational Heating Helps Make Massive Galaxies Red and Dead, Astrophys. J. Let. 697, 38 (2009)

Kennicutt, R.C., Star Formation in Galaxies Along the Hubble Sequence, Annu. Rev. Astron. Astrophys. 36, 189 (1998)

Leroy, A.K., The Star Formation Efficiency in Nearby Galaxies: Measuring Where Gas Forms Stars Effectively, Astron. J. 136, 2782 (2008)

Lianou, S., Xilouris, E., Madden, S., Barmby, P., The dustier early-type galaxies deviate from late-type galaxies' scaling relations, Mon. Not. R. Astron. Soc. 461, 2856 (2016)

Magdis, G. et al., The Evolving Interstellar Medium of Star-forming Galaxies since $z = 2$ as Probed by Their Infrared Spectral Energy Distributions, Astrophys. J. 760, 6 (2012)

Martig, M., Bournaud, F., Teyssier, R., Dekel, A., Morphological Quenching of Star Formation: Making Early-Type Galaxies Red, Astrophys. J. 707, 250 (2009)

Martig, M., Bournaud, F., Croton, D.J., Dekel, A., Teyssier, R., A Diversity of Progenitors and Histories for Isolated Spiral Galaxies, Astrophys. J. 756, 26 (2012)

Martig, M. et al., The ATLAS^{3D} project - XXII. Low-efficiency star formation in early-type galaxies: hydrodynamic models and observations

Saintonge, A. et al., COLD GASS, an IRAM legacy survey of molecular gas in massive galaxies - I. Relations between H_2, H I, stellar content and structural properties, Mon. Not. R. Astron. Soc. 415, 32 (2011)

Saintonge, A. et al., The Impact of Interactions, Bars, Bulges, and Active Galactic Nuclei on Star Formation Efficiency in Local Massive Galaxies, Astrophys. J. 758, 73 (2012)

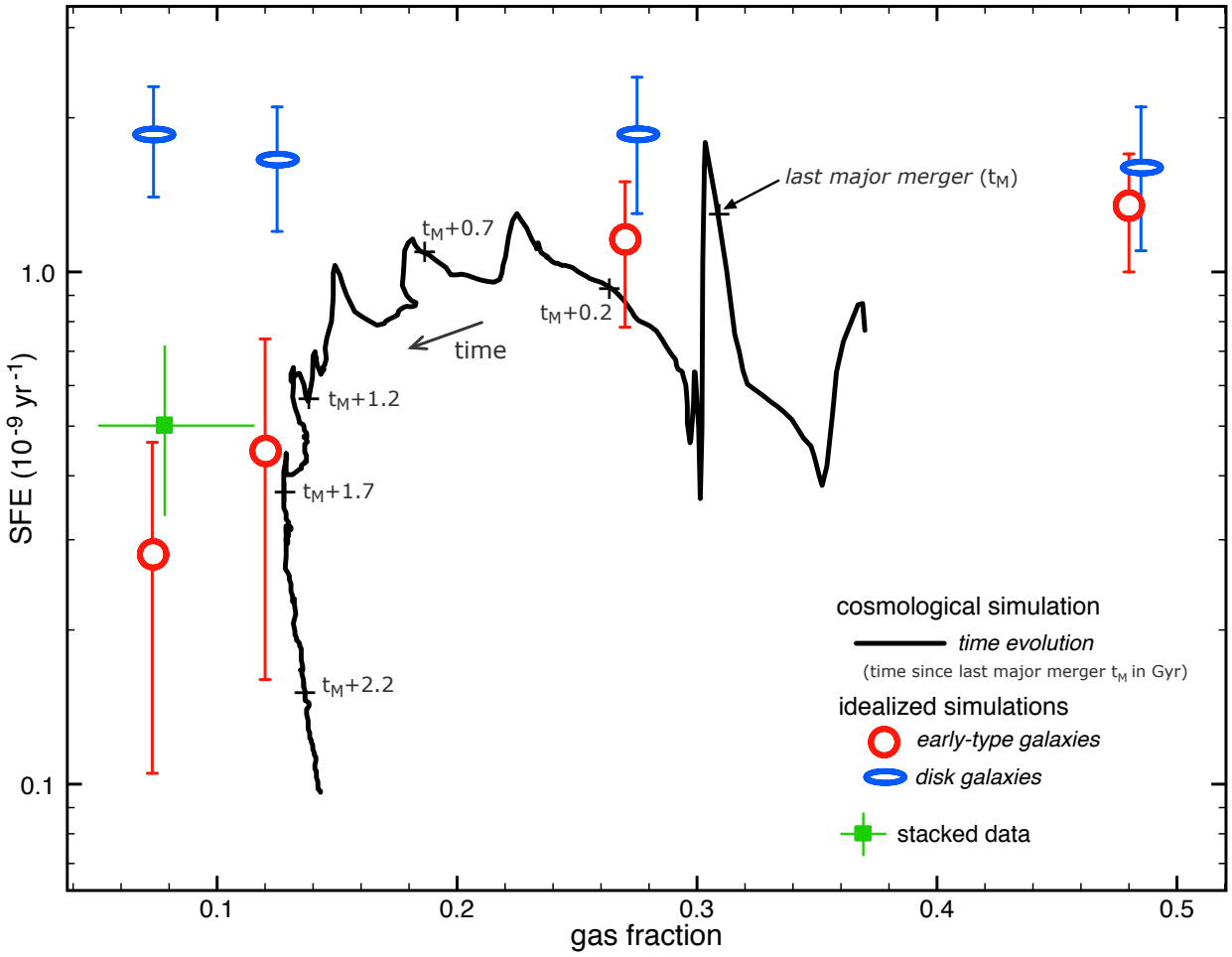

Figure 4: SFE as a function of gas fraction in high-resolution hydrodynamic simulations. The black line shows the evolutionary track of an ETG in a cosmological zoom-in simulation, with initial peaks of SFE corresponding to galaxy mergers, followed by gas consumption and a strong decrease of the SFE once the gas fraction gets lower than 20-25%. This effect, which has been dubbed "morphological quenching", does not occur in galaxies whose stellar structure remains disk-like (Martig et al., 2009). The galaxy already has an ETG morphology at the beginning of the track (Methods) but only quenches ~ 2 Gyr later when enough gas has been consumed. The red and blue symbols are from idealised simulations of galaxies of ETG and disk-dominated galaxies, respectively, where both gas structure and star formation are resolved at the parsec scale (Methods Martig et al., 2013). These confirm that the SFE drops below gas fractions of 20-25% only for ETGs, at a level consistent with our observations (filled green square).

Sargent, M.T. et al., Regularity Underlying Complexity: A Redshift-independent Description of the Continuous Variation of Galaxy-scale Molecular Gas Properties in the Mass-star Formation Rate Plane, Astrophys. J. 793, 19 (2014)

Sargent, M.T. et al., A Direct Constraint on the Gas Content of a Massive, Passively Evolving Elliptical Galaxy at z = 1.43, Astrophys. J. Let. 806, 20 (2015)

Smith, M.W. et al., The Herschel Reference Survey: Dust in Early-type Galaxies and across the Hubble Sequence, Astrophys. J. 748, 123 (2012)

Tacchella, S. et al., Evidence for mature bulges and an inside-out quenching phase 3 billion years after the Big Bang, Science 348, 314 (2015)

Tacconi, L.J. et al., Phibss: Molecular Gas Content and Scaling Relations in $z \sim 1-3$ Massive, Main-sequence Star-forming Galaxies, Astrophys. J. 768, 74 (2013)

Wuyts, S. et al., What Do We Learn from IRAC Observations of Galaxies at $2 < z < 3.5$?, Astrophys. J. 655, 51 (2007)

Methods

1 Conventions

Stellar masses and star formation rates (SFRs) derived from photometry assume a Salpeter (1955) stellar initial mass function, in accordance with the literature on IMF variations in ETGs (Grillo & Gobat, 2010; Cappellari et al., 2012; Conroy & van Dokkum, 2012). We assume for consistency the same IMF for galaxies on the main sequence of star formation (MS). For distances, cosmic times, and cosmological simulations, we assume a ΛCDM cosmology with $H_0 = 70$ km s^{-1} Mpc^{-1}, $\Omega_M = 0.3$, and $\Omega_\Lambda = 0.7$ (Larson et al., 2011; Planck, 2015).

2 Sample selection

We select galaxies from the COSMOS field (Scoville et al., 2007) using public UV-to-near infrared (NIR) photometry (Muzzin et al., 2013) and a new point-source-matched catalogue (Jin et al., in prep.; 8 μJy r.m.s.) based on public *Spitzer*/MIPS 24 μm data (Le Floc'h et al., 2009). We use spectroscopic redshifts from zCOSMOS (Lilly et al., 2007) when available and photometric redshifts (Muzzin et al., 2013) otherwise. Quiescent galaxies are first selected using both the *BzK* and high-redshift *UVJ* criteria (Daddi et al., 2004; Williams et al., 2009), which minimises the number of interlopers due to photometric uncertainties and highly-reddened star-forming galaxies. We then discard from the sample sources that are detected at $\geq 3\sigma$ significance in the 24 μm catalogue, which implies either significant star formation or AGN activity, and keep only galaxies with stellar masses higher than $\log M_\star = 10.8$ M$_\odot$ within uncertainties. This mass limit is chosen to ensure that the stellar mass distribution of this sample is similar to that of a spectroscopically observed subsample (Gobat et al., 2017, Supplementary Figure 1), for which accurate redshifts and stellar population parameters (age, SFR, metallicity) were estimated. It also corresponds to twice the completeness limit of the catalogue for $z > 1.5$ quiescent galaxies (Gobat et al., 2015). We also ignore possible galaxy pairs, i.e., with concordant redshifts (within $\Delta z_{\rm phot} \leq 0.2$) and separated by less than 60" ($\lesssim 30\%$ of the sample), to simplify the modelling of the far-infrared (FIR) emission (Supplementary Section 3). The final sample contains 977 pBzK+UVJp galaxies, with a median redshift of $\langle z \rangle = 1.76$ and a median stellar mass of $\langle M_\star \rangle = 1.1 \times 10^{11}$ M$_\odot$.

3 Far-infrared stack

The COSMOS survey includes imaging data at 24 μm (*Spitzer*/MIPS; Le Floc'h et al., 2009), 100 and 160 μm (*Herschel*/PACS, from the PEP survey; Lutz et al., 2011), 250, 350 and 500 μm (*Herschel*/SPIRE, from the HerMES survey; Oliver et al., 2012), 850 μm (JCMT/SCUBA2; Casey et al., 2013), 1.1 mm (ASTE/AzTEC; Aretxaga et al., 2011), and 1.4 GHz (VLA; Schinnerer et al., 2010). From these data we extract cutouts centred on each source in the sample with sizes 5 times larger than the beam FWHM. These are then combined to create a median 2D image in each band (Supplementary Figure 2), using a thousand bootstrap resamplings of the data with sizes of half the initial sample to estimate the variance of the sample. At each bootstrap iteration, the resulting median image is fit with a point source to estimate the central ETG flux. This measure is then corrected for clustering due to randomly distributed sources (Béthermin et al., 2015) while the contribution of the star-forming satellites of the ETGs is subtracted in two ways: if the beam size is smaller than the extension of the satellite halo (MIPS, PACS, 250 μm SPIRE, SCUBA-2, AzTEC, and VLA), a 2D satellite component multiplied by the normalised beam is added to the fit; alternatively (SPIRE 350 and 500 μm), an additional clustering correction is added representing the increasing fraction of flux coming from the satellites enclosed by the beam, with respect to the MIPS 24μm PSF one. In both cases, we use as reference the shape of the extinction-corrected SFR surface density profile of

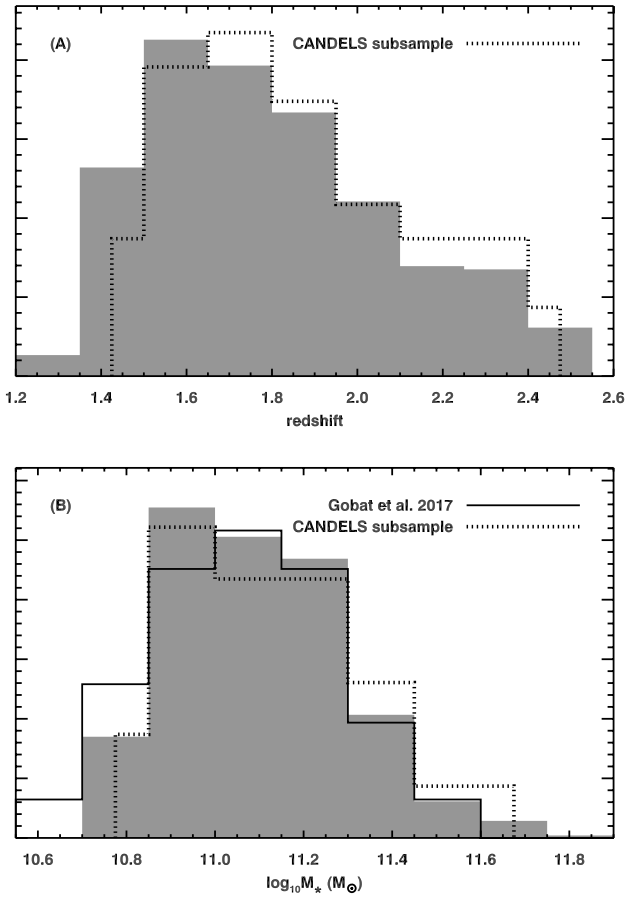

Figure 1: Distribution of photometric redshifts (A) and stellar masses (B) derived from UltraVISTA photometry. The solid histogram shows the distribution of the spectroscopic subsample from (Gobat et al., 2017), while the dotted one represents the distribution of sample ETGs in the CANDELS sub-field of COSMOS (see Supplementary Section 4).

satellites, modelled with a combination of a β-function and a multiplicative, two-parameter "quenching" term of the form $\min(r/r_q, 1)^{\alpha_q}$ (Supplementary Figure 3; for more information, see Gobat et al., 2015). We note that the satellite contributions at 850 μm (SCUBA-2) and 1.1 mm (AzTEC) estimated with second method are a factor ~3 higher than those derived from the decomposition, due to the lower dust temperature of the centrals' FIR emission. This also implies that the 350 and 500 μm SPIRE fluxes, for which we could not perform a 2D decomposition, might be slightly overestimated. The clustering-corrected fluxes and satellite corrections are given in Supplementary Table 1. These, and the total infrared luminosity $L_{\rm IR}$ we find, are a factor $\sim$ 3 higher than those inferred by Man et al. (2016) for quiescent galaxies at similar redshift and stellar mass. This difference could be accounted for by our strict selection and treatment of satellites. However, the Man et al. (2016) analysis used a different selection criterion and did not probe the Rayleigh-Jeans tail of the cold dust emission, which makes a more detailed comparison difficult.

The MIR and FIR emission from dust grains is then modelled with a set of Draine & Li (DL07 2007) templates, assuming $q_{\rm PAH} = 3.19\%$ and $U_{\rm max} = 10^6$ but with varying γ and $U_{\rm min}$, to estimate the total infrared luminosity $L_{\rm IR}$ and dust mass $M_{\rm dust}$. A detailed description of the model and of the fitting procedure is presented in (Magdis et al., 2012). On the other hand, the dust temperature $T_{\rm dust}$ is determined using a simple modified blackbody model (MBB) with a fixed effective emissivity $\beta = 1.8$. The derived parameter estimates are given in Supplementary Table 2. We note that $M_{\rm dust}$ estimates could vary substantially between a simple single-temperature MBB fit to the data and that of that of a full dust model like the one provided by DL07. However, when the adopted absorption cross section of the dust distribution ($\kappa_{\rm abs}$) used in the MBB model is consistent both in the normalisation and in the spectral index with that of the full dust model (DL07), the two techniques yield comparable results (e.g., Bianchi, 2013; Berta et al., 2016).

The major source of uncertainty in the derivation of $M_{\rm dust}$ is the appropriate value of $\kappa_{\rm abs}$, which remains unknown. However, the prescription used in the DL07 model provides $M_{\rm dust}$ (and therefore $M_{\rm gas}$) estimates that are consistent with independent gas measurements of star-forming galaxies at various redshifts (e.g., Magdis et al., 2012; Genzel et al., 2015). Furthermore, the DL07 model has been used to derive $M_{\rm gas}$ estimates for the comparison sample of local quiescent galaxies. Thus, our choice of the DL07 model for our analysis, even if the derived absolute value of $M_{\rm dust}$ ($M_{\rm gas}$) remains uncertain, facilitates the comparison between various local and high$-z$ samples and avoids any model dependent systematics.

Finally, we also add to the best-fit DL07 model a power-law radio slope with $\alpha = 0.8$ and a normalisation given by the FIR-radio correlation (Magnelli et al., 2015). The radio fluxes are however not included in the fit and both the data point and model are shown for reference only. We note that there appears to be a significant excess in the median flux at 1.4 GHz compared to the model, corresponding to $\sim 5 \times 10^{22}$ W/Hz. On the one hand, this is suggestive of the presence in our sample of low-excitation AGNs (Best & Heckman, 2012) and might be a sign of widespread, persistent AGN feedback. On the other hand, the normalisation of the FIR-radio correlation (FRC) has a dispersion of a factor $\sim$ 2 (Yun, Reddy & Condon, 2001), potentially lowering the significance of this excess. However, for an entire galaxy population to deviate from the median relation would imply that the slope and normalisation of the FRC vary significantly with, e.g., star formation efficiency (SFE) or specific SFR (sSFR), which is not substantiated by recent high-redshift studies (Ibar et al., 2009; Thomson et al., 2014; Magnelli et al., 2015).

3.1 Converting $M_{\rm dust}$ into $M_{\rm gas}$

While $M_{\rm dust}$ can be obtained directly from the FIR emission, the molecular gas mass $M_{\rm gas}$ is a more important quantity in the context of galaxy evolution. Since molecular hydrogen is essentially invisible, $M_{\rm gas}$ is usually extrapolated from other observables, either from sub-mm molecular (e.g., CO) line emission $M_{\rm dust}$, using conversion factors that are somewhat uncertain. In the case of $M_{\rm dust}$, a gas-to-dust ratio (G/D) is used, which is related to the gas-phase metallicity and to processes of dust creation and destruction. We use here $G/D \sim 95$, based on the parameterisation of the G/D as a function of metallicity from Magdis et al. (2012) and the assumption of solar metallicity for the gas in the ETGs, which is supported by two lines of indirect evidence: first, the average gas metallicity of star forming galaxies with the same sSFR is close to (or slightly above) the solar value, up to $z \sim 1.7$ (Mannucci et al., 2010; Kashino et al., 2017); second, a spectroscopic, rest-frame UV measurement of the metallicity of the last batch of stars in a subset of our ETG sample also yields $\sim Z_\odot$ (Gobat et al., 2017), the stellar metallicity being expected to be slightly lower, but otherwise comparable, to the gas one (Halliday et al., 2008).

The picture is however complicated by processes which can produce dust, such as supernovae, asymptotic giant-branch stars, or accretion of gas-phase metals in the ISM, and those that can destroy it (e.g., X-ray sputtering; Arimoto et al., 1997). While the bulk of cold dust in local ETGs does not appear to originate from stellar evolution (Smith et al., 2012; Agius et al., 2013), the G/D of ETGs might nonetheless not follow the same relations as MS galaxies. On the other hand, in local ETGs which have detected H_2 gas (i.e., the gas-rich population) the median G/D is significantly higher ($\sim$ 400), while in the undetected ones the median upper-limit on the G/D is slightly lower ($\sim$ 80) than our adopted value (Lianou et al., 2016). Overall, the global G/D of local ETGs appears to follow a similar relation to that of star-forming galaxies (Leeuw et al., 2008; Smith et al., 2012; Lianou et al., 2016).

Finally, we make the simplification that all the hydrogen gas in our distant ETGs is in molecular (H_2) form, rather than atomic (HI) or a mix of both. We base this assumption on the high H_2/HI ratios seen in local ETGs (Crocker et al.,

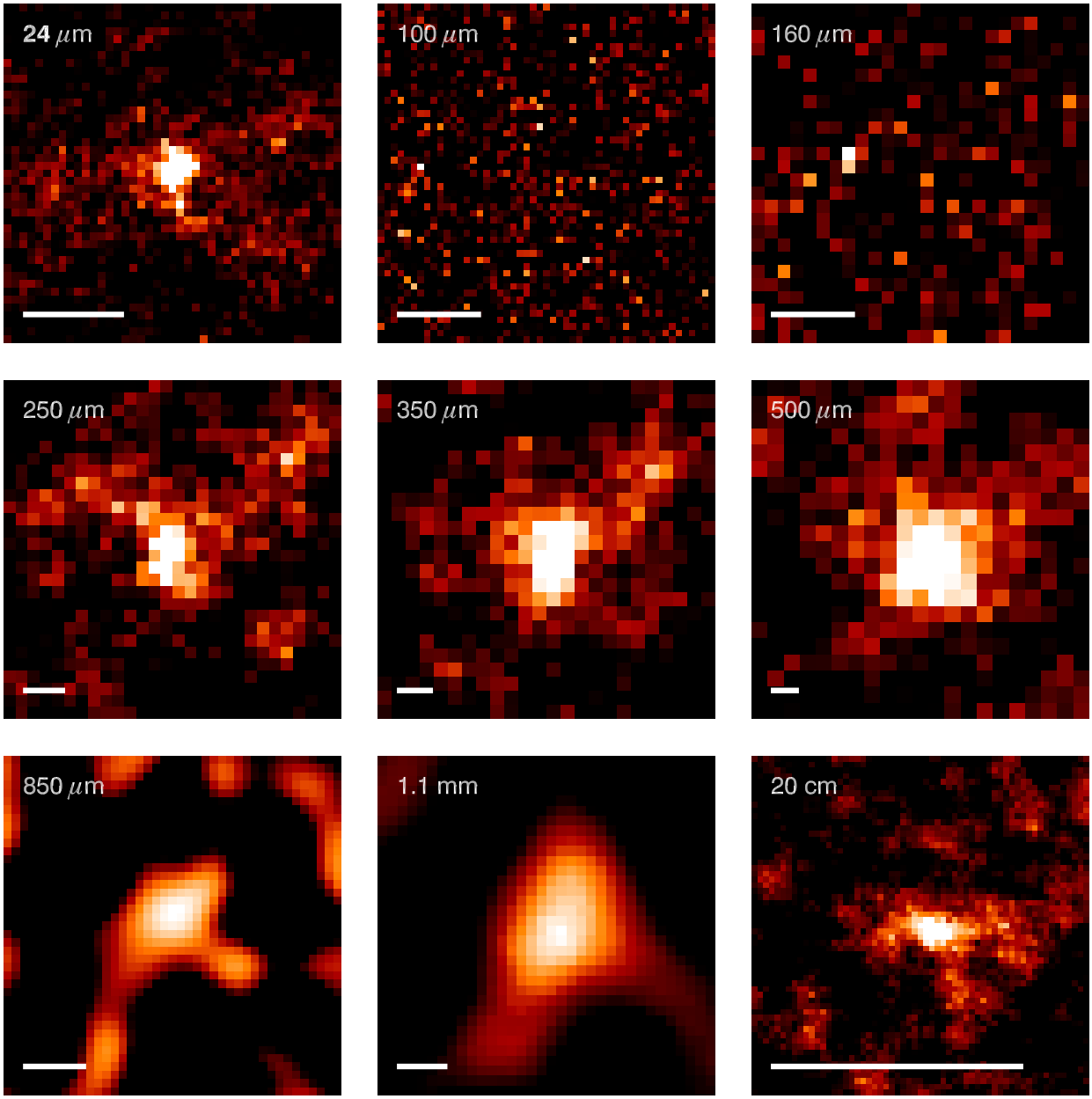

Figure 2: Median stacked cutouts at the position of the pBzK+UVJp galaxies, at 24 μm (*Spitzer/MIPS*), 100 and 160 μm (*Herschel*/PACS), 250, 350 and 500 μm *Herschel*/SPIRE, 850 μm (JCMT/SCUBA-2), 1.1 mm (ASTE/AzTEC) and 1.4-3 GHz (JVLA). All cutouts are shown with the same relative flux scale and the white bar in each panel has a length of 15".

Table 1: Corrected MIR, FIR, and radio fluxes of the $z \sim 1.76$ ETGs derived from median stacking, in μJy *(top)*, and fraction of flux in the beam emitted by satellites, in *% (bottom)*.

24 μm	100 μm	160 μm	250 μm	350 μm	500 μm	850 μm	1.1 cm	22 cm
6.9 ± 0.6	60 ± 25	53 ± 22	268 ± 36	339 ± 39	296 ± 26	81 ± 23	57 ± 16	3.7 ± 0.8
30	40	50	55	60	65	10	5	< 20

Table 2: Far-infrared properties derived from the stacked FIR emission of the $z \sim 1.76$

log $L_{\rm IR}$ [a]	SFR[b]	$\langle U \rangle$[c]	$T_{\rm dust}$[d]	log $M_{\rm dust}$[e]	log $M_{\rm gas}$[f]	log $M_\star$[g]	$f_{\rm gas}$[h]
$L_\odot$	$M_\odot$ yr^{-1}		K	$M_\odot$	$M_\odot$	$M_\odot$	
10.46 ± 0.14	$4.8^{+1.8}_{-1.3}$	2.2 ± 1.1	22.6 ± 2	8.00 ± 0.2	9.98 ± 0.2	11.08 ± 0.09	$7.4^{+4.6}_{-3.0}$%

[a] Total IR luminosity integrated from 8 to 1000 μm. [b] Star formation rate. [c] Mean starlight intensity. [d] Dust temperature. [e] Dust mass. [f] Hydrogen gas mass (see Methods). [g] Stellar mass. [h] Gas fraction, $M_{\rm gas}/(M_\star + M_{\rm gas})$

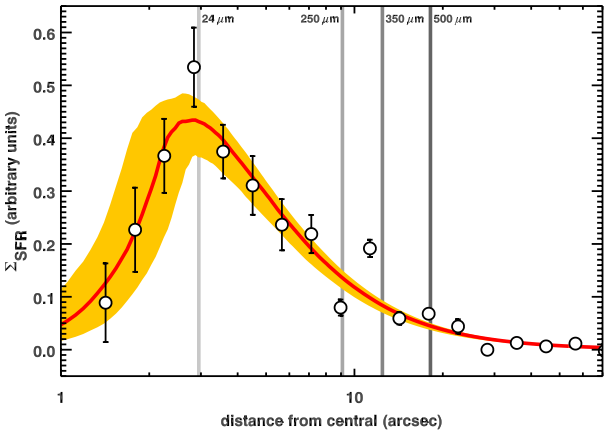

Figure 3: Average SFR surface density profile of the satellites of $z \sim 1.76$ ETGs. The red line and yellow shaded region show the best-fit "quenched" β-model, with uncertainties. The grey vertical lines show the half-width at half-maximum of the instruments' beams from 24 μm to 500 μm.

2011; Davis et al., 2015). This ratio appears nevertheless to vary substantially in the local population (Welch, Sage & Young, 2010), possibly as a result of differential evolution, with lenticular (S0) galaxies containing higher amounts of H_2 (Sage, Welch & Young, 2007). We note that, while high-redshift quiescent galaxies tend to have a more disky morphology (i.e., closer to S0s) than local ETGs (Chevance et al., 2012; Krogager et al., 2014; Bruce et al., 2014, see also Supplementary Section 4), the cold gas in local S0s is likely to have a different origin than that of high-redshift ETGs.

4 Morphologies

There exist several publicly available high-resolution imaging datasets on the COSMOS field, taken with the *Hubble Space Telescope* (HST). The most extensive was obtained with the *Advanced Camera for Surveys* and covers 1.7 degrees at 814 nm (Koekemoer et al., 2007), corresponding to rest-frame UV wavelengths at $z > 1.4$. This implies that *HST*/ACS imaging might, for this sample, trace the younger stars produced by the last significant star formation episode more than the total stellar mass distribution. Moreover, the existence of morphological gradients in high-redshift ETGs is well attested (Guo et al., 2011; Gargiulo et al., 2012; Chan et al., 2016). Here we therefore use the much smaller CANDELS survey (Koekemoer et al., 2011), which benefits from NIR (i.e., rest-frame optical) data at 1.2 and 1.6 μm. We select the 46 ETGs in our sample whose position overlaps with the *HST*/WFC3 mosaics of the CANDELS survey (a random selection of which is shown in Supplementary Figure 4), as well as 12 medium luminosity stars ($14 < V < 16$) in the same region. We extract cutouts around the targets from both the F125W and F160W images and combine them using the same method as in Supplementary Section 3, to generate median NIR images of the galaxies and point sources. These are then used in conjunction with the `galfit` code (Peng et al., 2010) and fitted with a Sérsic profile. This yields a Sérsic index of $n = 3.5 \pm 0.1$ and effective radius of $r_e = 1.7 \pm 0.1$ kpc, consistent with spheroidal morphology and on the stellar mass-size relation for early-type galaxies at this redshift (Mancini et al., 2010; van der Wel, 2014). The results of this morphological modelling are shown in Supplementary Figure 5. Furthermore, 40 of these galaxies have individually measured morphologies in the van der Wel (2014) catalog, with median values of $n \sim 3$ and $r_e \sim 1.3$ kpc, respectively. Similar results and high Sérsic indices are also found for the full sample; more details will be presented in a future publication.

5 Hydrodynamical simulations

The cosmological simulation used in this work (Figure 4) is performed in a zoom box focusing on a massive galaxy at the centre of its dark matter halo. The size of the box corresponds to twice the virial radius of the dark halo, without boundary conditions for mass infall. The latter is based on a large-scale cosmological simulation. The simulation of a forming ETG analysed here is from Martig et al. (2009), with a complete sample presented in Martig et al. (2012). The evolution of the morphology of both its gas and star components is shown in Supplementary Figure 6. The galaxy starts as disk dominated at high redshift ($z > 1.5$), then undergoes a series of mergers with mass ratios ranging from 10:1 to 3:1. These mergers have two effects: they convert the stellar structure into a spheroid and compress the gas, increasing the star formation and gas consumption rates. Over the 3 Gyr long track used in Figure 4, the stellar morphology is consistently spheroidal, although sometimes disturbed by mergers in their early stages. Over this period, the stellar mass increases from $\sim 6 \times 10^{10}$ $M_\odot$ to 1.2×10^{11} $M_\odot$, consistent with our observed sample. About 40% of this increase comes from star formation internal to the studied galaxies, while the rest is accreted during mergers with other, smaller galaxies.

The idealised simulations are performed with the Adaptive Mesh Refinement code RAMSES (Teyssier, 2002). They are similar to those presented in Martig et al. (2013), but have double the resolution, reaching 3 pc in the densest gas regions (see also Sargent et al., 2015). The gas fraction coverage has been extended with new simulations, fully identical to the previous ones for all other parameters. These idealised simulations do not follow the formation of a given galaxy in a cosmological context. Instead, the stellar and gas mass, as well as their spatial distributions, are arbitrarily chosen to be representative of a certain type of galaxy. The simulations reach a very high resolution in order to accurately describe the fragmentation of gas in the dense clouds where stars form (see discussion in Martig et al., 2013). They also allow for direct comparisons of the SFE between disk-dominated galaxies and ETGs, with all other parameters being identical. The error bars in Figure 4 correspond to the r.m.s. fluctuation of the SFE between various snapshots of a given simulation. The agreement between these idealised simulations and the cosmological

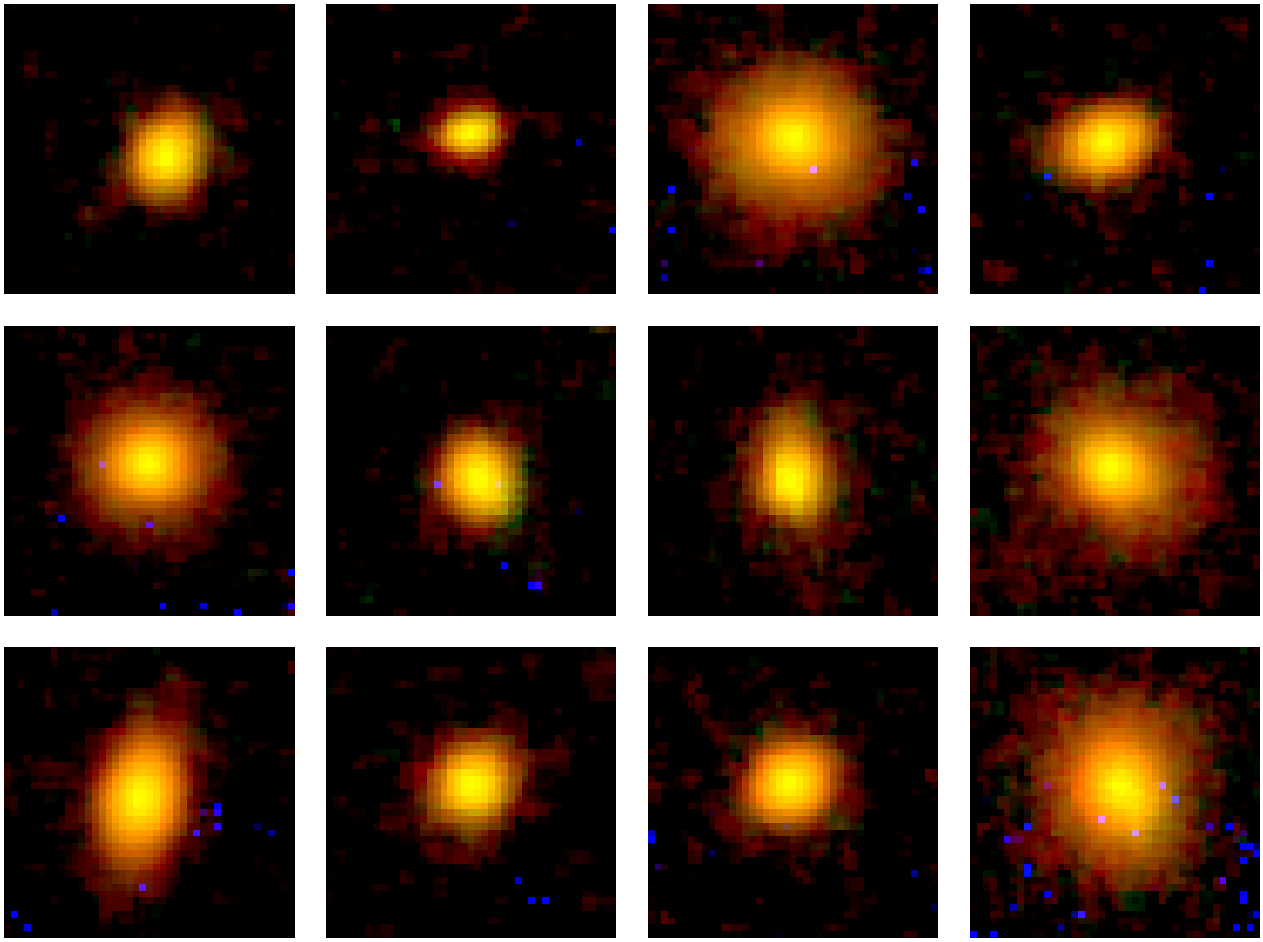

Figure 4: RGB-composite (*HST*/WFC3 F160W, F125W, F606W) cutout images of sample ETGs in the CANDELS (Koekemoer et al., 2011) field. The F125W and F606W images have been smoothed with a Gaussian kernel to match the resolution of the F160W data. Each cutout is 2.4" (or ∼20 kpc) on the side.

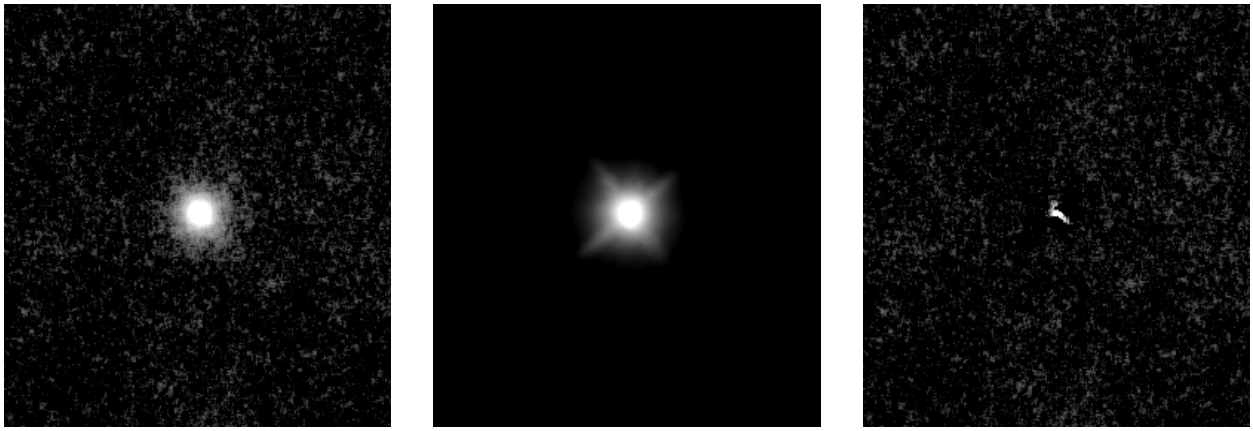

Figure 5: Median *HST*/WFC3 F160W stack of the ETGs in the CANDELS field (left), with best-fit Sérsic model (centre) and residuals after subtraction (right), for the same scale and limits.

simulation confirms that the process highlighted in the cosmological simulation is not redshift-dependent: while the reduction of the SFE in a spheroid-dominated galaxy (once enough gas has been consumed) happens at about redshift $z \sim 1$ in this simulation, it can just as well occur at somewhat higher redshift, as in our observations. Finally, we note that the idealised simulations do not include diffuse gas reservoirs in the galaxies' outskirts, yielding slightly higher values of the SFE than the cosmological simulation by normalising the SFR to slightly lower gas masses.

6 Gas return rate

The amount of gas returned to the ISM by a stellar population depends on both its IMF and the star formation history (SFH). It is generally among the parameters estimated by stellar population synthesis models for single age populations (SSP; Bruzual & Charlot, 2003; Maraston, 2005). The typical mass-weighted age of *BzK*-selected quiescent galaxies inferred from spectroscopy is $t_{SF} = 2 - 3$ Gyr (Onodera et al., 2015; Gobat et al., 2017). We assume a delayed, exponentially declining SFH, arbitrarily starting at $z = 10$, as the simple parametric form that is closest to the probable "true" SFH of these high-redshift ETGs (rising as the galaxy grows on or above the MS, then decreasing during quenching). In this case, the SFH that would reproduce the SFR inferred from the cold dust emission has $t_{SF} \sim 2.24$ Gyr. The amount of gas returned to the ISM over a certain time span can then be computed easily as the convolution of the SFH and mass loss function due to stellar death. For our chosen SFH and IMF, this would amount to 37^{+2}_{-1}% of the observed stellar mass at $z = 1.76$ and, given the median stellar mass of ETGs in this sample, an average return rate of $1.3^{+1.6}_{-1.3}$ $M_\odot$ yr^{-1} over the last 500 Myr. We note that single burst or truncated SFHs, also commonly used in spectral and photometric modelling, would yield similar total gas fractions but negligible return rates at $z = 1.76$.

7 X-ray stacking

We use deep X-ray observations of the COSMOS field by the *Chandra* and *XMM-Newton* observatories (Finoguenov et al., 2007; Elvis et al., 2009) to constrain the total mass of the halos hosting our sample ETGs. This procedure is similar to that described in Béthermin et al. (2014) and Gobat et al. (2015), and we refer to these articles for additional information. There are 585 sample ETGs in the *Chandra* COSMOS Survey field and located in zones free from emission. After subtracting both background and point sources, we find a residual flux in the 0.5-2 keV band of $(2.3 \pm 0.6) \times 10^{-17}$ erg cm^{-2} s^{-1}, corresponding to a luminosity of $L_X = (5.1 \pm 1.3) \times 10^{42}$ erg cm^{-2} s^{-1} and a mass of $M_{200c} = (1.2 \pm 0.2) \times 10^{13}$ $M_\odot$.

Acknowledgements

The new simulations presented in this work were performed on GENCI resources (allocations 2016-04-2019 and 2017-04-2192).

References

Agius, N.K. et al., GAMA/H-ATLAS: linking the properties of submm detected and undetected early-type galaxies - I. $z \leq 0.06$ sample, Mon. Not. R. Astron. Soc. 431, 1929 (2013)

Aretxaga, I. et al., AzTEC millimetre survey of the COSMOS field - III. Source catalogue over 0.72 deg^2 and plausible boosting by large-scale structure, Mon. Not. R. Astron. Soc. 415, 3831 (2011)

Berta, S., Lutz, D., Genzel, R., Förster-Schreiber, N.M., Tacconi, L.J., Measures of galaxy dust and gas mass with Herschel photometry and prospects for ALMA, Astron. Astrophys. 587, 73 (2016)

Best, P.N., Heckman, T.M., On the fundamental dichotomy in the local radio-AGN population: accretion, evolution and host galaxy properties, Mon. Not. R. Astron. Soc. 421, 1569 (2012)

Béthermin, M. et al., Clustering, host halos, and environment of $z \sim 2$ galaxies as a function of their physical properties, Astron. Astrophys. 567, 103 (2014)

Bianchi, S., Vindicating single-T modified blackbody fits to Herschel SEDs, Astron. Astrophys. 552, 89 (2013)

Bruce, V.A. et al., The bulge-disc decomposed evolution of massive galaxies at $1 < z < 3$ in CANDELS, Mon. Not. R. Astron. Soc. 444, 1001 (2014)

Bruzual, G., Charlot, S., Stellar population synthesis at the resolution of 2003, Mon. Not. R. Astron. S. 344, 1000 (2003)

Cappellari, M. et al., Systematic variation of the stellar initial mass function in early-type galaxies, Nature 484, 485 (2012)

Casey, C.M. et al., Characterization of SCUBA-2 450 μm and 850 μm selected galaxies in the COSMOS field, Mon. Not. R. Astron. Soc. 436, 1919 (2013)

Chan, J.C.C. et al., Sizes, colours gradients and resolved stellar mass distributions for the massive cluster galaxies in XMMUJ2235-2557 at $z = 1.39$, Mon. Not. R. Soc. 458, 3181 (2016)

Chevance, M. et al., On the Shapes and Structures of High-redshift Compact Galaxies, Astrophys. J. Let. 754, 24 (2012)

Conroy, C., van Dokkum, P.G., The Stellar Initial Mass Function in Early-type Galaxies From Absorption Line Spectroscopy. II. Results, Astrophys. J. 760, 71 (2012)

Davis, T.A. et al., Molecular and atomic gas in dust lane early-type galaxies - I. Low star formation efficiencies in minor merger remnants, Mon. Not. R. Astron. Soc. 449, 3505 (2015)

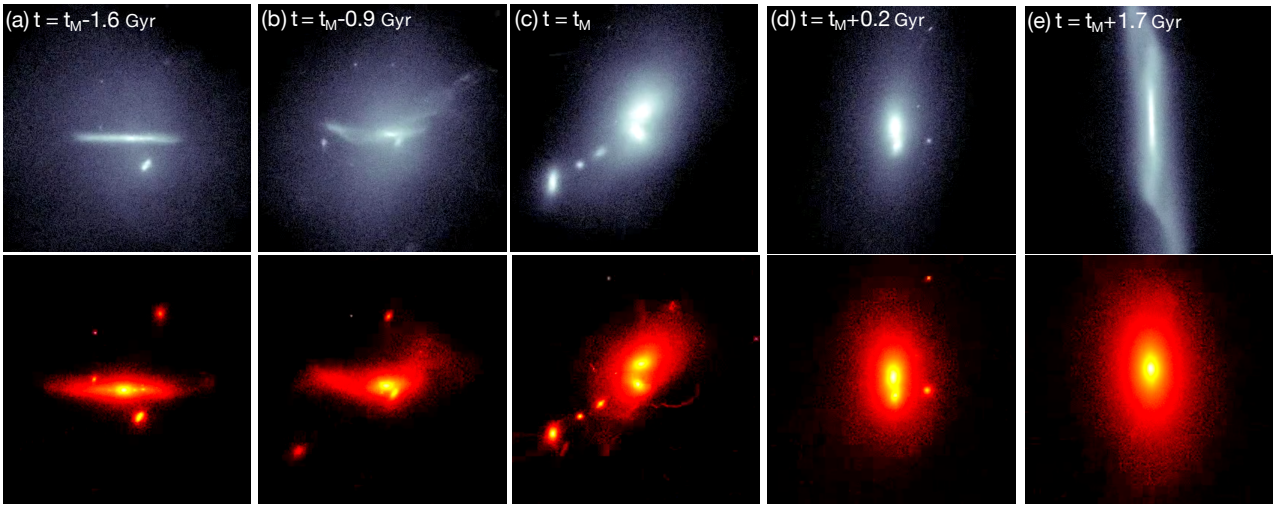

Figure 6: The cosmological simulation analysed here (Martig et al., 2009) models the formation and evolution of an ETG. Starting disk-dominated at redshifts $z \sim 2$ and above (a), this galaxy experiences several mergers that disrupt its stellar disk (b) and convert it into a spheroid, with the last significant mergers shortly before z=1 (c). The mergers compress the gas toward the centre (d), inducing bursts of star formation and gas consumption and reducing the gas fraction to about 20%. The gas then rapidly settles back in a thin rotating disk, but the lack of gravitational coupling to a co-rotating stellar disk quenches star formation with a SFR 5-10 times lower than in a spiral galaxy with the same gas content (e). The captions show the gas (top) and star (bottom) surface density at different redshift, over sizes of 20×20 kpc.

Elvis, M. et al., The Chandra COSMOS Survey. I. Overview and Point Source Catalog, Astrophys. J. Supp. S. 184, 158 (2009)

Finoguenov, A. et al., The XMM-Newton Wide-Field Survey in the COSMOS Field: Statistical Properties of Clusters of Galaxies, Astrophys. J. Supp. S. 172, 128 (2007)

Gargiulo, A., Saracco, P., Longhetti, M., La Barbera, F., Tamburri, S., Spatially resolved colours and stellar population properties in early-type galaxies at $z \sim 1.5$, Mon. Not. R. Soc. 425, 2698 (2012)

Genzel, R. et al., Combined CO and Dust Scaling Relations of Depletion Time and Molecular Gas Fractions with Cosmic Time, Specific Star-formation Rate, and Stellar Mass, Astrophys. J. 800, 20 (2015)

Gobat, R., Satellite content and quenching of star formation in galaxy groups at $z \sim 1.8$, Astron. Astrophys. 581, 56 (2015)

Grillo, C., Gobat, R., On the initial mass function and tilt of the fundamental plane of massive early-type galaxies, Mon. Not. R. Astron. Soc. Let. 402, 64 (2010)

Guo, Y. et al., Color and Stellar Population Gradients of Passively Evolving Galaxies at $z \sim 2$ from HST/WFC3 Deep Imaging in the Hubble Ultra Deep Field, 2011, Astrophys. J. 735, 18 (2011)

Halliday, C. et al., GMASS ultradeep spectroscopy of galaxies at $z \sim 2$. I. The stellar metallicity, Astron. Astrophys. 479, 417 (2008)

Ibar, E., Deep multi-frequency radio imaging in the Lockman Hole using the GMRT and VLA - I. The nature of the sub-mJy radio population, Mon. Not. R. Astron. Soc. 397, 281 (2009)

Kashino, D. et al., The FMOS-COSMOS Survey of Star-forming Galaxies at $z \sim 1.6$. IV. Excitation State and Chemical Enrichment of the Interstellar Medium, Astrophys. J. 835, 88

Koekemoer, A.M. et al., The COSMOS Survey: Hubble Space Telescope Advanced Camera for Survey Observations and Data Processing, Astrophys. J. Supp. S. 172, 196 (2007)

Koekemoer, A.M. et al., CANDELS: The Cosmic Assembly Near-infrared Deep Extragalactic Legacy Survey - The Hubble Space Telescope Observations, Imaging Data Products, and Mosaics, Astrophys. J. Supp. S. 197, 36 (2011)

Krogager, J.-K., Zirm, A.W., Toft, S., Man, A., Brammer, G., A Spectroscopic Sample of Massive, Quiescent $z \sim 2$ Galaxies: Implications for the Evolution of the Mass-Size Relation, Astrophys. J. 797, 17 (2014)

Larson, D. et al., Seven-year Wilkinson Microwave Anisotropy Probe (WMAP) Observations: Power Spectra and WMAP-derived Parameters, Astrophys. J. Supp. S. 192, 16 (2011)

Leeuw, L.L., Davidson, J., Dowell, C.D., Matthews, H.E., Spatially Resolved Imaging at 350 μm of Cold Dust in Nearby Elliptical Galaxies, Astrophys. J. Let. 677, 249 (2008)

Le Floc'h, E. et al., Deep Spitzer 24 μm COSMOS Imaging. I. The Evolution of Luminous Dusty Galaxies - Confronting the Models, Astrophys. J. 703, 222 (2009)

Lilly, S.J. et al., zCOSMOS: A Large VLT/VIMOS Redshift Survey Covering $0 < z < 3$ in the COSMOS Field, Astrophys. J. Supp. S. 172, 70 (2007)

Lutz, D. et al., PACS Evolutionary Probe (PEP) - A Herschel key program, Astron. Astrophys. 532, 90 (2011)

Magnelli, B. et al., The far-infrared/radio correlation and radio spectral index of galaxies in the SFR-$M_\star$ plane up to $z \sim 2$, Astron. Astrophys. 573, 45 (2015)

Man, A.W.S. et al., Confirming the Existence of a Quiescent Galaxy Population out to $z = 3$: A Stacking Analysis of Mid-, Far-Infrared and Radio Data, Astrophys. J. 820, 11 (2016)

Mancini, C., et al., High-redshift elliptical galaxies: are they (all) really compact ?, Mon. Not. R. Astron. Soc. 401, 933 (2010)

Mannucci, F., Cresci, G., Maiolino, R., Marconi, A., Gnerucci, A., A fundamental relation between mass, star formation rate and metallicity in local and high-redshift galaxies, Mon. Not. R. Astron. Soc. 408, 2115 (2010)

Maraston, C., Evolutionary population synthesis: models, analysis of the ingredients and application to high-z galaxies, Mon. Not. R. Astron. Soc. 362, 799 (2005)

Muzzin, A. et al., A Public K_s-selected Catalog in the COSMOS/ULTRAVISTA Field: Photometry, Photometric Redshifts, and Stellar Population Parameters, Astrophys. J. Supp. S. 206, 8 (2013)

Oliver, S.J. et al., The Herschel Multi-tiered Extragalactic Survey: HerMES, Mon. Not. R. Astron. Soc. 424, 1614 (2012)

Onodera, M. et al., The Ages, Metallicities, and Element Abundance Ratios of Massive Quenched Galaxies at $z \geq 1.6$, Astrophys. J. 808, 161 (2015)

Peng, C.Y., Ho, L.C., Impey, C.D., Rix, H.-W., Detailed Decomposition of Galaxy Images. II. Beyond Axisymmetric Models, Astron. J. 139, 2097 (2010)

Planck Collaboration et al., Planck 2015 results. XIII. Cosmological parameters, Astron. Astrophys. 594, 13 (2015)

Sage, L.J., Welch, G.A., Young, L.M., The cool ISM in elliptical galaxies. I. A survey of molecular gas, Astrophys. J. 657, 232 (2007)

Salpeter, E.E., The Luminosity Function and Stellar Evolution, Astrophys. J. 121, 161 (1955)

Scoville, N. et al., The Cosmic Evolution Survey (COSMOS): Overview, Astrophys. J. Supp. S. 172, 1 (2007)

Schinnerer, E. et al., The VLA-COSMOS Survey. IV. Deep Data and Joint Catalog, Astrophys. J. Supp. S. 188, 384 (2010)

Teyssier, R., Cosmological hydrodynamics with adaptive mesh refinement. A new high resolution code called RAMSES, Astron. Astrophys. 385, 337 (2002)

Thomson, A.P. et al., An ALMA survey of submillimetre galaxies in the Extended *Chandra* Deep Field South: radio properties and the far-infrared/radio correlation, Mon. Not. R. Astron. Soc. 442, 577 (2014)

van der Wel, A., 3d-HST+CANDELS: The Evolution of the Galaxy Size-Mass Distribution since $z = 3$, Astrophys. J. 788, 28 (2014)

Welch, G.A., Sage, L.J., Young, L.M., The cool interstellar medium in elliptical galaxies. II. Gas content in the volume-limited sample and results from the combined elliptical and lenticular surveys, Astrophys. J. 725, 100 (2010)

Williams, R.J., Quadri, R.F., Franx, M., van Dokkum, P., Labbé, I., Detection of Quiescent Galaxies in a Bicolor Sequence from $z = 0 - 2$, Astrophys. J. 691, 1879 (2009)

Yun, M.S., Reddi, N.A., Condon, J.J., Radio Properties of Infrared-selected Galaxies in the IRAS 2 Jy Sample, Astrophys. J. 554, 803 (2001)